Sonic Anemometer as a small Acoustic Tomography Array

Sergey N. Vecherin · Vladimir E. Ostashev · Christopher W. Fairall · D. Keith Wilson · Ludovic Bariteau

---

S.N. Vecherin · V.E. Ostashev · D.K. Wilson

U.S. Army Engineer Research and Development Center, 72 Lyme Road, Hanover, NH 0375, USA

V.E. Ostashev · L. Bariteau

Cooperative Institute for Research in Environmental Sciences, University of Colorado at Boulder, 325 Broadway, Boulder, CO 80305-3337, USA

C.W. Fairall

NOAA/Earth System Research Laboratory, 325 Broadway, Boulder, CO 80305-3337, USA

Abstract

Sonic anemometers are widely used for measurements of temperature and velocity. The spatial resolution of a sonic anemometer is limited by the distance between its transducers. For studies of small-scale turbulence and theories of turbulence, it is desirable to increase this spatial resolution. To this end, in this paper, it is suggested to modify a sonic anemometer by considering it as a small acoustic tomography array and applying appropriate inverse algorithms for reconstruction of temperature and velocity. A particular modification of the sonic is considered when the number of its transducers is doubled and the recently developed time-dependent stochastic inversion algorithm is used for reconstruction. Numerical simulations of the sonic anemometer and its suggested modification are implemented with the temperature and velocity fields modelled as the quasi-wavelets moving through the sonic's volume. It is shown that the suggested modification of the sonic anemometer enables better reconstruction of temperature and velocity than the sonic does. Furthermore, the spatial resolution of the temperature and vertical velocity spectra is increased by a factor of 10. The spatial resolution in the suggested modification of the sonic is determined by the size of the computational grid and can be increased with increasing number of transducers.

Keywords Acoustic tomography · Sonic anemometer · Spatial resolution ·

1 Introduction

Sonic anemometers are robust instruments for measurements of temperature and velocity and have been used for such measurements for many decades, e.g., Kaimal and Finnigan (1994). Due to concerns about wind distortion, transducers of a sonic anemometer should be located at some distance from each other. As a result, a sonic enables path-averaged measurements of temperature and velocity. Horst and Oncley (2006) reviewed currently used sonic anemometers. It follows from their paper that the path averaging lengths of the sonic anemometers are in the range of $0.12-0.2$ m. Such path averaging does not allow studies of small-scale turbulence in the inertial range which extends to a few mm in the atmosphere. Studies of small-scale turbulence have been recently of interest for physics of the atmospheric surface layer (ASL) and theories of turbulence (e.g., Fairall et al., 2003, Chamecki and Dias, 2004). In principle, hot-wire and cold-wire anemometers enable one to make measurements of small-scale turbulence. However, these anemometers are not reliable instruments and often brake down. Furthermore, they might disturb the flow around them. Therefore, it would be desirable to modify currently used sonic anemometers for measurements of small-scale turbulence. The main goal of the present paper is to study a feasibility of using a sonic anemometer as a small acoustic tomography array to increase the spatial resolution in measurements of temperature and velocity.

The ultrasound travel-time tomography has been used for many years in medicine and technology for reconstructing the image of a medium through which the ultrasound waves propagate. In these fields, the number of ultrasound propagation paths usually greatly exceeds

the number of unknown parameters of the medium so that tomographic reconstruction is an overdetermined inverse problem.

The first experimental implementation of acoustic travel-time tomography of the ASL was done by Wilson and Thomson (1994). In this case, the number of sound propagation paths is usually less than the number of temperature and wind velocity values to be reconstructed at selected points within the tomographic region so that one deals with an underdetermined inverse problem. To solve this problem, the time-dependent stochastic inversion (TDSI) algorithm was recently developed and successfully applied to reconstruction of the temperature T and wind velocity $\mathbf{v}$ fields in acoustic tomography experiments (Vecherin et al. 2006, Vecherin et al. 2008). The current status of acoustic tomography of the ASL is reviewed in Ostashev et al. (2009).

In this paper, it is suggested to consider a sonic anemometer as a small acoustic tomography array and use appropriate inverse algorithms for reconstruction of the fine structure of the T and $\mathbf{v}$ fields inside the sonic. A particular modification of the sonic is studied when the number of its transducers is doubled and the TDSI algorithm is used for tomographic reconstruction. Numerical simulations of temperature and velocity measurements with the sonic anemometer and its suggested modification are implemented. In the simulations, the T and $\mathbf{v}$ fields inside the sonic and its modification are modeled with quasi-wavelets (QWs). The QWs are eddy-like structures of temperature and velocity which are convenient representation of turbulence at small scales (Wilson et al. 2009). The numerical simulations will allow us to compare the errors in measurements of temperature and velocity with the sonic anemometer and its

suggested modifications, and the spatial resolutions with which the spectra of temperature and velocity fluctuations are obtained.

The paper is organized as follows. In Sec. 2, the geometry and principle of operation of the sonic anemometer and its suggested modification are considered. In Sec. 3, the results of numerical simulations are presented and discussed. Section 4 summarizes the results obtained in the paper.

2 Sonic anemometer and its suggested modification

2.1 Sonic anemometer

Though a design of sonic anemometers varies substantially, their principle of operation is similar and can be understood by considering, for example, the CSAT3 sonic anemometer shown in Fig. 1. There are 3 transducers at both the "upper" and "lower" levels of the sonic which point downwards and upwards, respectively. In numerical simulations of the sonic anemometer, we will assume that the upper and lower transducers are separated in the vertical direction by 0.2 m. These transducers form three sound propagation paths, marked as a, b, and c, whose elevation angles with respect to a horizontal plane are 60°. The projections of these paths on the horizontal plane located in the middle of the sonic intersect at 120°. The transducers serve alternately as sources (transmitters) and receivers. As a result, the sound pulses propagate in the opposite directions (i.e., upward and downward) of each path thus enabling measurements of six travel times τ_i of sound propagation between transducers. Here, $i = 1, 2, ..., N$, where

$N = 6$.

The adiabatic sound speed (e.g., see Ostashev, 1997, Sec. 6.1.3) $c = \sqrt{\gamma_a R_a T}$ and the wind velocity vector $\mathbf{v} = (v_x, v_y, v_z)$ are assumed to be constant within the sonic anemometer. Here, $\gamma_a = 1.40$ is the ratio of specific heats for dry air, R_a the gas constant for dry air, T the acoustic virtual temperature, which, hereinafter, is referred to as temperature, and v_x, v_y, v_z are the velocity components in the Cartesian coordinate system (x, y, z). The sound speed c and, hence, the temperature T, are determined from a sum of the travel times τ_i of sound propagation along the opposite directions of, e.g., the path a. The projections of the velocity vector $\mathbf{v}$ on the paths a, b, and c are determined from the differences of the travel times τ_i of sound propagation along opposite directions of these paths, respectively. From these projections, it is straightforward to calculate v_x, v_y, and v_z. The corresponding formulas can be found in Kaimal and Finnigan (1994), and CSAT3 sonic instruction manual (1998). The spatial resolution of a sonic anemometer is limited by path averaging, i.e., the assumption that T, v_x, v_y, and v_z are constant along sound propagation paths between transducers.

2.2 Sonic anemometer as a tomography array

A suggested modification of the sonic anemometer is shown in Fig. 2. There are 6 transducers at both the upper and lower levels so that the number of transducers is doubled in comparison with a sonic. The lower and upper level transducers are located along the perimeter of a square with the side length of 0.1m and are separated in the vertical direction by 0.2 m, i.e., the same distance as in the considered above sonic anemometer.

In Fig. 2, each transducer works alternately as a source and receiver. We also assume that each transducer at the lower level can receive signals from every transducer at the upper level, and visa versa. This increases the number of sound propagation paths to $6 \times 6 = 36$. Taking into account that sound signals can propagate in opposite directions of each path, the total number of the travel times τ_i which can be measured with this modification of the sonic anemometer is $N = 72$.

2.3 Time-dependent stochastic inversion

In the considered modification of the sonic anemometer, reconstruction of the temperature $T(\mathbf{R}, t)$ and velocity $\mathbf{v}(\mathbf{R}, t)$ fields is done with the TDSI algorithm. Here, $\mathbf{R} = (x, y, z)$ are the Cartesian coordinates and t is time. It is convenient to express these fields in the following form: $T(\mathbf{R}, t) = T_0(t) + T_1(\mathbf{R}, t)$ and $\mathbf{v}(\mathbf{R}, t) = \mathbf{v}_0(t) + \mathbf{v}_1(\mathbf{R}, t)$, where the subscripts "0" and "1" correspond to the mean fields (i.e., the fields averaged over the tomographic volume) and their fluctuating parts, respectively. The mean fields $T_0(t)$ and $\mathbf{v}_0(t)$ are reconstructed from the measured travel times $\tau_i(t)$ using the least-square estimation. The temperature $T_1(\mathbf{R}, t)$ and velocity $\mathbf{v}_1(\mathbf{R}, t)$ fluctuations are reconstructed with the TDSI algorithm.

The main idea of the TDSI algorithm is to assume that the temperature and velocity fluctuations are random fields with the known spatial-temporal correlation functions $B_T(\mathbf{R}, t)$ and $B_{nm}(\mathbf{R}, t)$, respectively, where $n, m = 1, 2, 3$. These correlation functions are usually chosen as the Gaussian homogeneous and isotropic correlation functions whose characteristic lengths by the order of magnitude determine the smallest scales of temperature and velocity which can

be resolved in reconstruction. To implement this idea, the travel times $\tau_i(t_j)$ are repeatedly measured at the time moments t_j, where $j = 1, 2, ..., M$, and, then, used in reconstruction of the temperature and velocity fluctuations.

The input parameters in the least-square estimation of the mean fields, T_0 and $\mathbf{v}_0$, and the TDSI algorithm for reconstruction of the fluctuations, T_1 and $\mathbf{v}_1$, are the travel times $\tau_i(t_j)$ of sound propagation, the distances between transducers, and the variances and correlation lengths of $B_T(\mathbf{R}, t)$ and $B_{nm}(\mathbf{R}, t)$ (the latter two are needed for TDSI). The total fields $T(\mathbf{R}, t) = T_0(t) + T_1(\mathbf{R}, t)$ and $\mathbf{v}(\mathbf{R}, t) = \mathbf{v}_0(t) + \mathbf{v}_1(\mathbf{R}, t)$ and the estimated errors in their reconstruction are calculated with equations derived in Vecherin et al. (2006). Numerical simulations and acoustic tomography experiments showed that this approach enables accurate reconstruction of the temperature and velocity fields, e.g., see Ostashev et al. (2009).

3 Numerical simulations

3.1 Reconstruction of temperature and velocity fields

In numerical simulations, the temperature and velocity fields inside the sonic anemometer and its modification were modeled as QWs. The smallest and largest QWs had sizes of 0.01 m and 2 m, respectively. The size of the computational grid along the x, y, and z-axes was equal to the smallest QW, i.e., 0.01 m. The QW temperature and velocity fields were created in the volume of 20 m $\times$ 0.1 m $\times$ 0.2 m. In the simulations, this volume was moving in the direction of the x-axis with the velocity $U = 2$ m/s; the total time of the numerical experiment was (20 m) /

(2 m/s) = 10 s. Figure 3 shows a snapshot of the temperature and three components of the velocity fields inside the sonic anemometer and its suggested modification obtained with QWs. In the numerical simulations, the discretization time was 0.005 s so that the total number of snapshots of the T and $\mathbf{v}$ fields was 2000. For each snapshot, the travel times τ_i along all sound propagation paths in the sonic anemometer (Fig. 1) and its suggested modification (Fig. 2) were calculated.

The travel times τ_i for the sonic anemometer and formulas known in the literature (e.g., Kaimal and Finnigan, 1994) were, then, used to calculated the path-averaged values of temperature and velocity. The obtained time series of T, v_z, v_x, and v_y are depicted as red lines in the left plots in Figs. 4 - 7, respectively. The blue lines are the QW values of T, v_z, v_x, and v_y in the center of the sonic anemometer. The agreement between these QW values and the path-averaged values of T, v_z, v_x, and v_y reconstructed in numerical simulations of the sonic is relatively good. The root-mean square errors (RMSEs) between the red and blue lines in the left plots in Figs. 4 - 7 are $\sigma_T^s = 0.090$ °C, $\sigma_{v_z}^s = 0.056$ m/s, $\sigma_{v_x}^s = 0.086$ m/s, and $\sigma_{v_y}^s = 0.083$ m/s, respectively. Here, the superscript "s" stands for "sonic". The RMSE for the vertical velocity, $\sigma_{v_z}^s$ is about 1.5 times smaller than the RMSEs for the horizontal components of the velocity, $\sigma_{v_x}^s$ and $\sigma_{v_y}^s$. This is due to the fact that the sound propagation paths in the sonic anemometer have relatively large elevation angles of 60° so that the vertical velocity, v_z is reconstructed more accurately than the horizontal components, v_x and v_y. If desired, this condition can be relaxed by making the elevation angles of sound propagation paths close to 45°.

Then, the travel times τ_i for the considered modification of the sonic were used as input parameters for reconstruction of the mean and fluctuating parts of the temperature and velocity fields. In the TDSI algorithm for reconstruction of the fluctuations, three consequent values of the travel times τ_i were employed. Furthermore, the square roots of the variances of the spatial-temporal correlation functions of temperature and three components of velocity fluctuations were calculated for the considered QW field and were 0.074 °C, 0.057 m/s, 0.058 m/s, and 0.064 m/s, respectively; the correlation length of these fluctuations was $L_{T,v} = 0.03$ m. In the right plots in Figs. 4 - 7, the time series of the reconstructed values of T, v_z, v_x, and v_y in the center of the considered modification of the sonic are shown as red lines, respectively. The blue lines are again the QW values of T, v_z, v_x, and v_y in the center of the sonic, i.e., the blue lines in the left and right plots in these figures are the same. It follows from the right plots in Figs. 4 - 7 that the agreement between the QW and reconstructed values of T, v_z, v_x, and v_y is very good and is better than for the sonic (see left plots). The RMSEs between the QW and reconstructed values of T, v_z, v_x, and v_y are smaller than those for the sonic: $\sigma_T = 0.75\sigma_T^s = 0.067$ °C, $\sigma_{v_z} = 0.62\sigma_{v_z}^s = 0.035$ m/s, $\sigma_{v_x} = 0.91\sigma_{v_x}^s = 0.077$ m/s, and $\sigma_{v_y} = 0.85\sigma_{v_y}^s = 0.070$ m/s, respectively.

The results of the numerical simulations shown in Figs. 4 - 7 clearly indicate that the suggested modification of the sonic anemometer enables more accurate reconstruction of temperature and vertical velocity, and somewhat better reconstruction of the horizontal velocity. These results are used in the next subsection to study reconstruction of the spectra of temperature and velocity fluctuations with the sonic anemometer and its modification.

3.2 Spectra of temperature and velocity fluctuations

The time series T, v_z, v_x, and v_y obtained in numerical simulations of the sonic anemometer and its suggested modification and plotted in Figs. 4 - 7 were employed to calculate the mean values of temperature and three components of the velocity and their fluctuating parts. The fluctuations were then used to calculate the 1D spectra $S(k)$ of temperature and velocity, where k is the turbulence wavenumber. These spectra, normalized by the corresponding QW spectra $S_0(k)$, are plotted in Fig. 8. The red and blue lines correspond to the sonic anemometer and its modification, respectively. For a perfect reconstruction when the ratio $S(k)/S_0(k) = 1$, these solid lines would coincide with the black, horizontal lines also plotted in the figures.

It follows from the upper two plots in Fig. 8 that the sonic anemometer enables correct reconstruction of both the temperature and vertical velocity spectra for the wavenumbers k smaller than about 13 rad/m. This corresponds to the spatial scales of turbulence larger than 0.23 m which is the distance between the transducers in the sonic anemometer used in the numerical simualtions (see Fig. 1). Thus, the numerical simulations confirm that the sonic anemometer enables measurements of temperature and velocity spectra at spatial scales larger than or equal to the distance between its transducers.

On the other hand, as one can see in the upper two plots in Fig. 8, the suggested modification of the sonic anemometer enables correct reconstruction of the temperature and vertical velocity spectra for k smaller than about 130 rad/m, thus increasing its spatial resolution by a factor of ten. These values of k correspond to the spatial scales of turbulence larger than 0.02 m. This spatial scale is equal to the doubled grid size which is the maximum spatial resolution

according to the Nyquist theorem. Thus, the spatial resolution of the suggested modification of the sonic anemometer is determined by the size of the computational grid, which, in its turn, is determined by the number of transducers, their geometry, and the inverse algorithm for reconstruction of the temperature and velocity fields.

The normalized spectra of the horizontal velocity components, v_x, and v_y, reconstructed in numerical simualtions of the sonic anemometer and its modification are shown in the lower two plots in Fig. 8, respectively. It follows from these figures that the reconstructed spectra significantly deviate from the QW spectra in the range $k \gtrsim 10$ rad/m and that the reconstruction accuracy is about the same for the sonic anemometer and its modification. These results are due to predominantly vertical orientations of the sound propagation paths for both the sonic anemometer and its modification, when the horizontal components of the velocity are reconstructed less accurately than the vertical component.

4 Conclusions

To increase the spatial resolution of a sonic anemometer, it was suggested to consider it as a small acoustic tomography array and apply appropriate inverse methods for reconstruction of the temperature and velocity fields. A particular modification of the sonic anemometer was studied when the number of its transducers is doubled and reconstruction of the temperature and velocity fields is done with the recently developed time-dependent stochastic inversion (TDSI) algorithm. Numerical simulations of the sonic anemometer and its suggested modifi-

cation were implemented with the temperature and velocity fields modeled as quasi wavelets (QWs). The simulations showed that the sonic anemometer enables measurements of the time series of temperature and velocity with relatively small root-mean square errors (RMSE)s. The suggested modification of the sonic allows even more accurate measurements, especially for temperature and the vertical component of velocity when the corresponding RMSEs are smaller than those for the sonic by factors 0.75 and 0.62, respectively. The increase in accuracy is less pronounced for the horizontal components of velocity due to predominantly vertical orientations of the ultrasound propagation paths in the sonic anemometer and its modification.

The main advantage of the considered modification of the sonic anemometer is a significant increase in the spatial resolution of the spectra of temperature and vertical velocity fluctuations. The numerical simulations showed that the sonic anemometer enables correct measurements of these spectra up to the inverse of the distance between its transducers. This result clearly indicates the effect of path-averaging on the measurements of the spectra. On the other hand, the considered modification of the sonic enables correct reconstruction of these spectra up to the wavenumbers by an order of magnitude larger than those for the sonic. Its spatial resolution is determined by the size of the computational grid which relates to the number of transducers, their geometry, and the inverse algorithm for reconstruction.

From a technological point of view, the considered modification of the sonic anemometer seems feasible. Other modifications might also be feasible with more transducers at the upper and lower levels. With increased number of transducers, the spatial resolution can be further increased. Also, the inverse problem in reconstruction of temperature and velocity might be-

come overdetermined so that standard inverse algorithms (e.g., the least-square estimation) can be employed.

Acknowledgements This material is based upon work supported by the U.S. Army Research Laboratory and Army Research Office under contract/grant number W911NF1010415. Dr. Vecherin's work was performed during an appointment to the Postgraduate Research Participation Program at the U. S. Army Cold Regions Research and Engineering Laboratory (CRREL) administrated by the Oak Ridge Institute for Science and Education (ORISE) through an interagency agreement between the U. S. Department of Energy and CRREL.

References

Chamecki M, Dias NL (2004) The local isotropy hypothesis and the turbulent kinetic energy dissipation rate in the atmospheric surface layer. Q J R Meteorol Soc 130:2733-2752

CSAT3 three dimensional sonic anemometer instruction manual (1998). Campbell Scientific, Inc.

Fairall CW, Bradley EF, Hare JE, Grachev AA, Edson JB (2003) Bulk parametrization of air-sea fluxes: Updates and verification of the COARE algorithm. J Climate 16:571-591

Horst TW, Oncley SP (2006) Corrections to intertial-range power spectra measured by CSAT3 and solent sonic anemometers, 1. Path-averaging errors. Boubdary-Layer Meteorol 119:375-395

Kaimal JC, Finnigan JJ (1994) Atmospheric boundary layerflows-Their structure and measurement. University Press, Oxford

Ostashev VE (1997) Acoustics in Moving Inhomogeneous Media. E & FN SPON London

Ostashev VE, Vecherin SN, Wilson DK, Ziemann A, Goedecke GH (2009) Recent progress in acoustic travel-time tomography of the atmospheric surface layer. Meteorol Zeitschrift 18:125-133

Vecherin SN, Ostashev VE, Goedecke GH, Wilson DK, Voronovich AG (2006) Time-dependent stochastic inversion in acoustic travel-time tomography of the atmosphere. J Acoust Soc Am 119:2579-2588

Vecherin SN, Ostashev VE, Wilson DK, Ziemann A (2008) Time-dependent stochastic inversion in acoustic tomography of the atmosphere with reciprocal transmission. Meas Sci Technol 19

Wilson DK, Thomson DW (1994) Acoustic tomographic monitoring of the atmospheric surface

layer. J Atmos Ocean Tech 11:751-769

Wilson DK, Ostashev VE, Goedecke GH (2009) Quasi-wavelet formulations of turbulence and other random fields with correlated properties. Probabilistic Engineering Mechanics 24:343-357

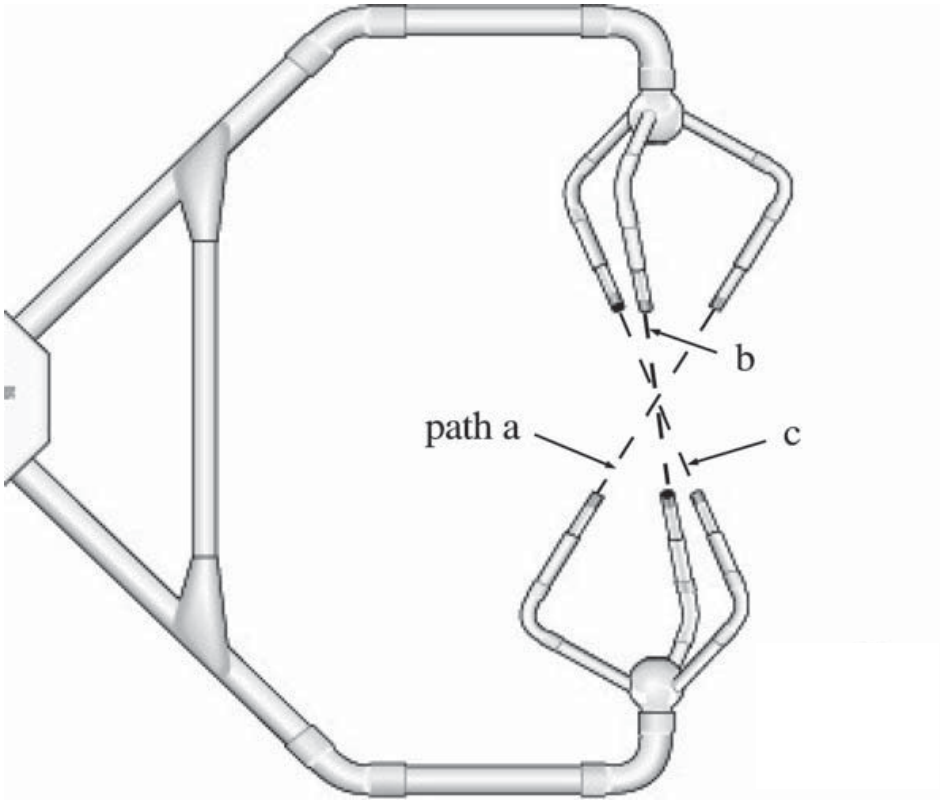

Figure 1: Schematic of CSAT3 sonic anemometer. The ultrasound propagation paths a, b, and c are shown as dashed lines.

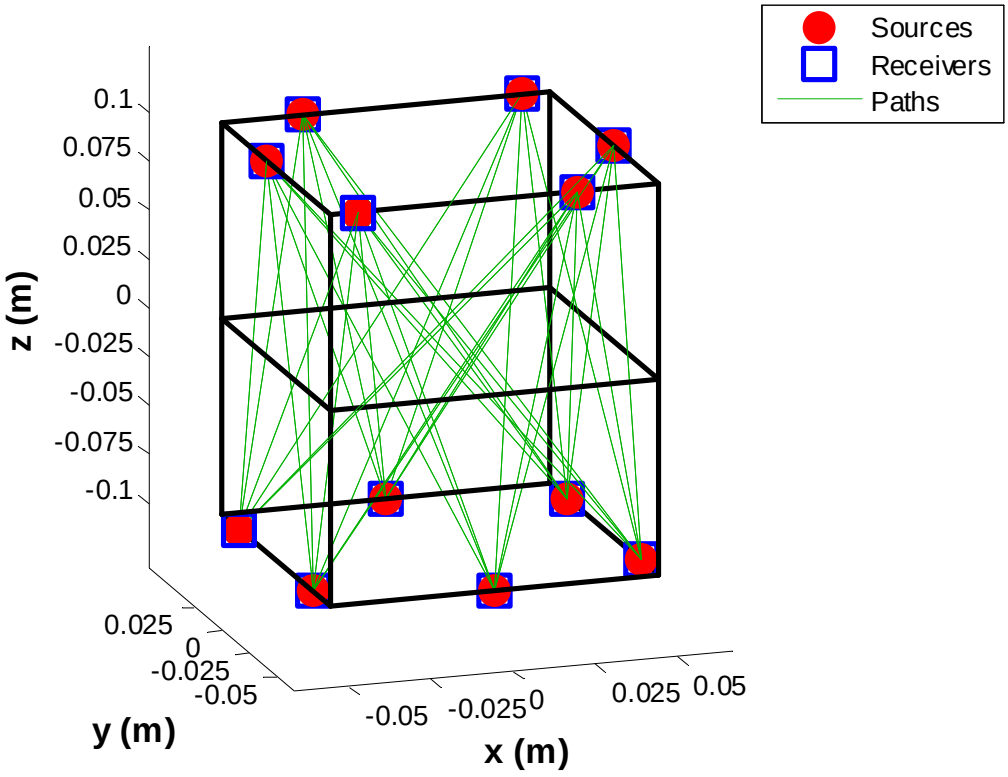

Figure 2: Schematic of the suggested modification of the sonic anemometer. Transducers at the upper ($z = 0.1$m) and lower ($z = -0.1$ m) levels work alternately as ultrasound sources and receivers. Green lines are the ultrasound propagation paths between transducers.

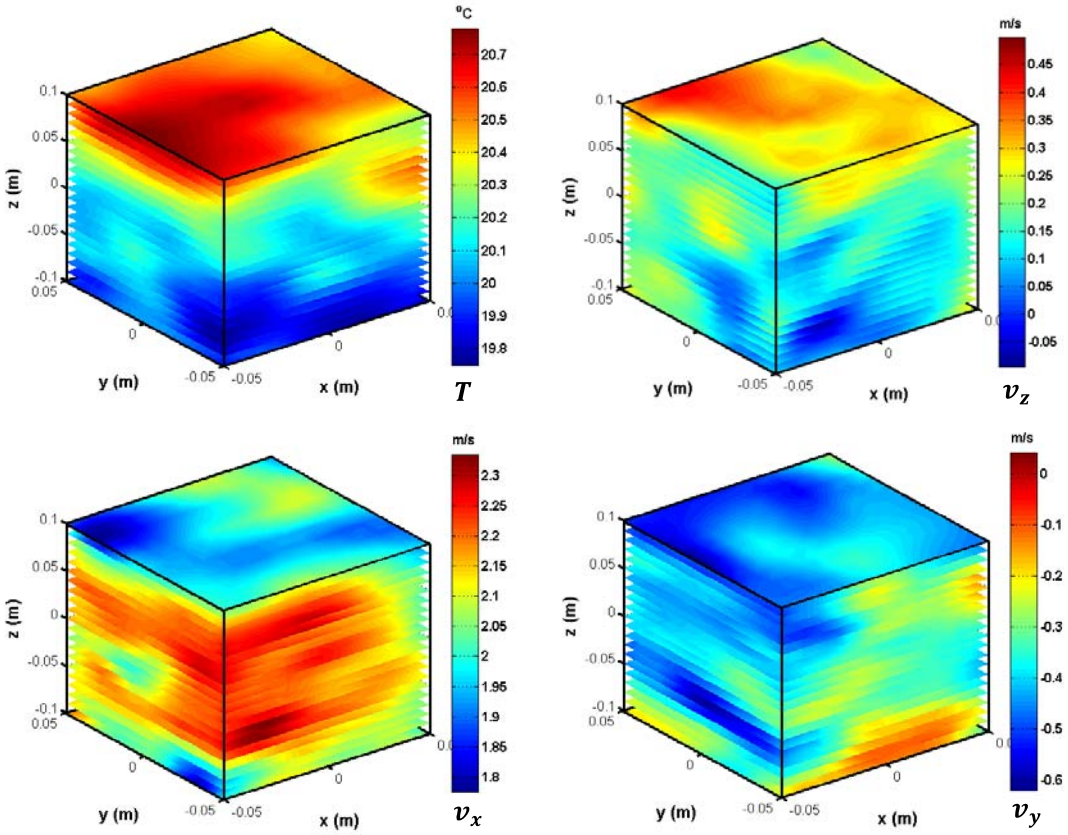

Figure 3: Snapshot of the temperature and three components of the velocity fields obtained with quasi-wavelets. (Upper left) $T(x, y, z)$, (upper right) $v_z(x, y, z)$, (lower left) $v_x(x, y, z)$, and (lower right) $v_y(x, y, z)$.

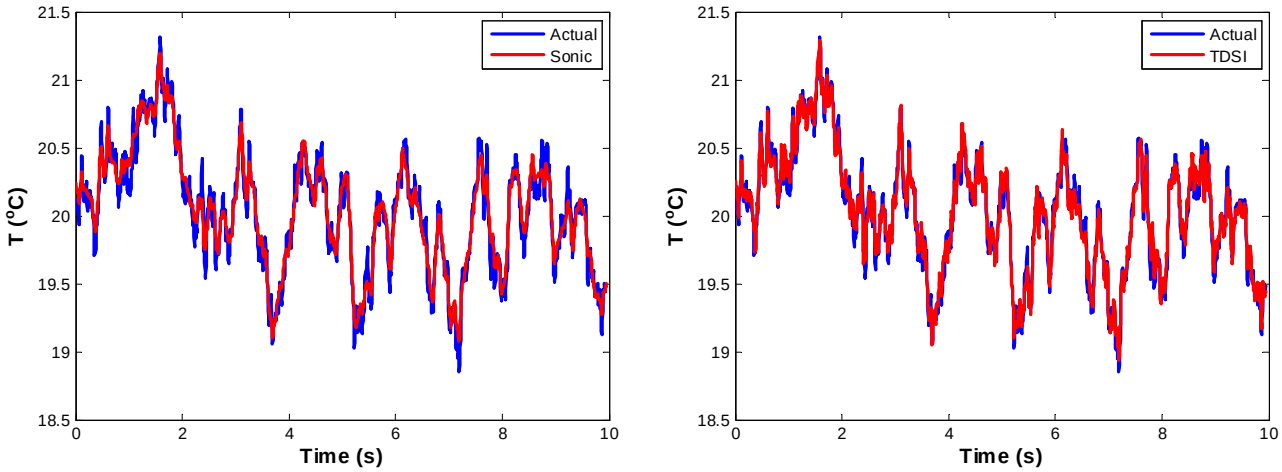

Figure 4: Time series of temperature, $T(t)$. Blue lines are the QW values of temperature in the center of the sonic anemometer and its suggested modification. Red lines are the values of temperature reconstructed in numerical simulations of the sonic (left plot) and its modification (right plot).

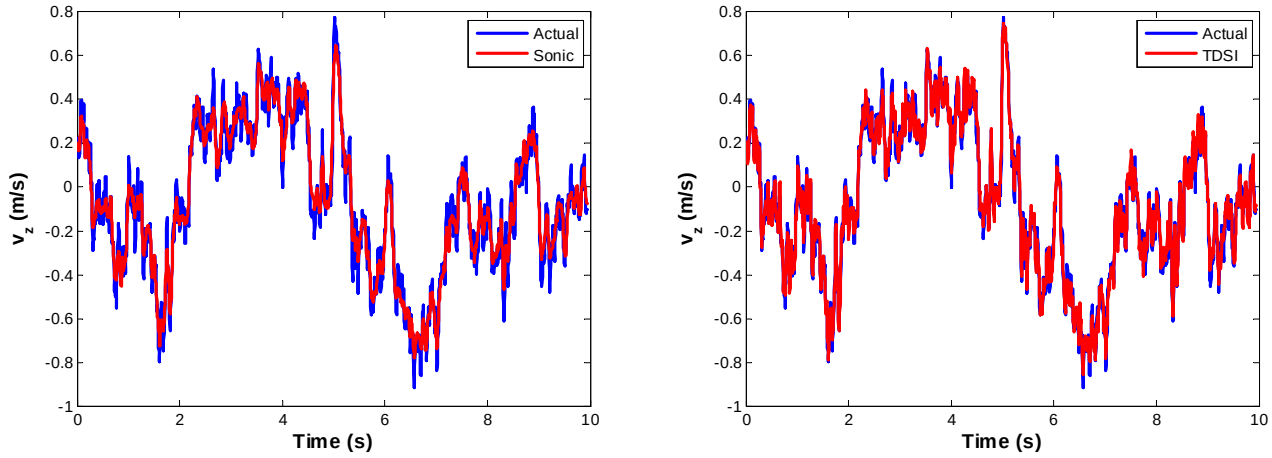

Figure 5: Time series of the vertical component of the velocity, $v_z(t)$. Blue lines are the QW values of v_z in the center of the sonic anemometer and its suggested modification. Red lines are the values of v_z reconstructed in numerical simulations of the sonic (left plot) and its modification (right plot).

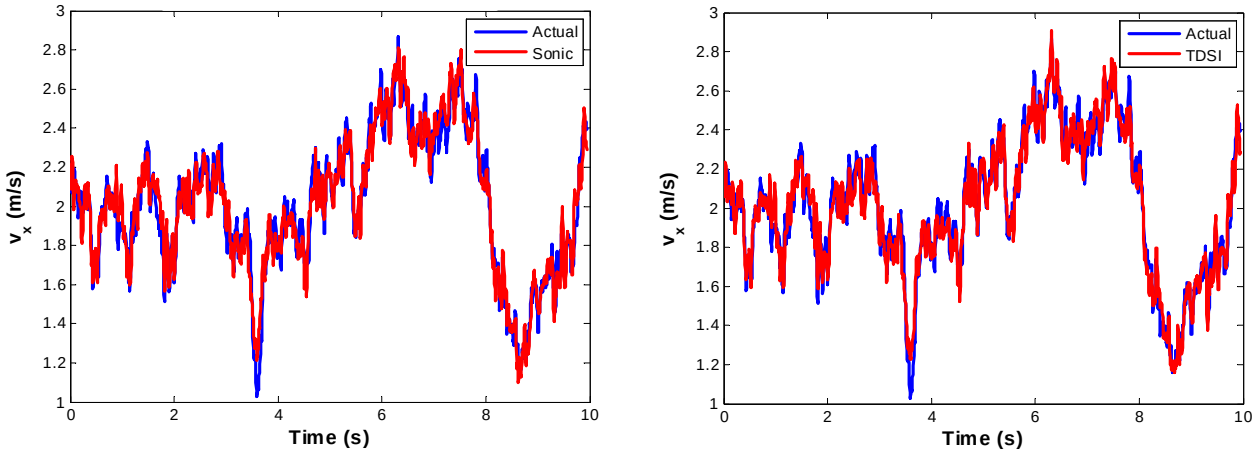

Figure 6: Time series of the x-component of the horizontal velocity, $v_x(t)$. Blue lines are the QW values of v_x in the center of the sonic anemometer and its suggested modification. Red lines are the values of v_x reconstructed in numerical simulations of the sonic (left plot) and its modification (right plot).

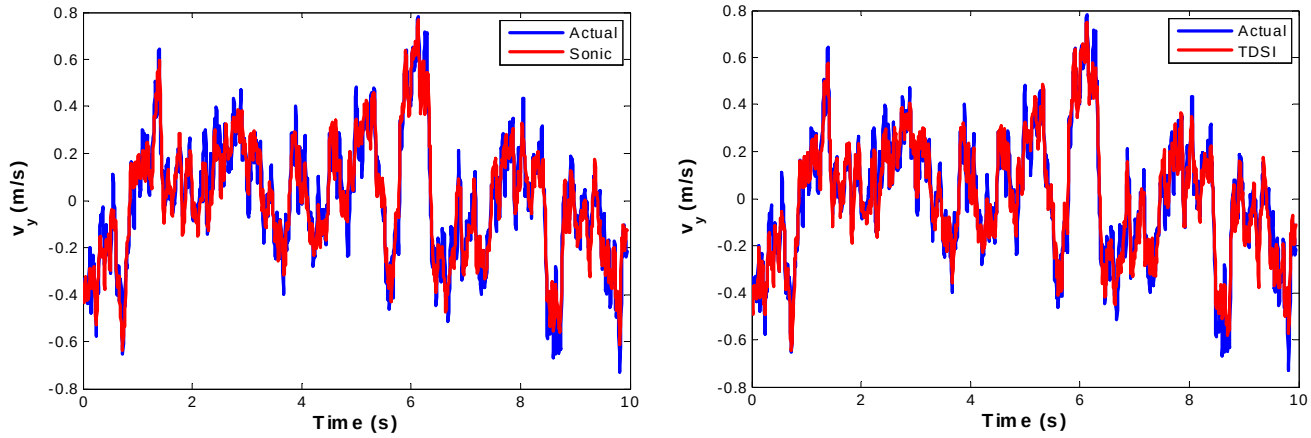

Figure 7: Time series of the y-component of the horizontal velocity, $v_y(t)$. Blue lines are the QW values of v_y in the center of the sonic anemometer and its suggested modification. Red lines are the values of v_y reconstructed in numerical simulations of the sonic (left plot) and its modification (right plot).

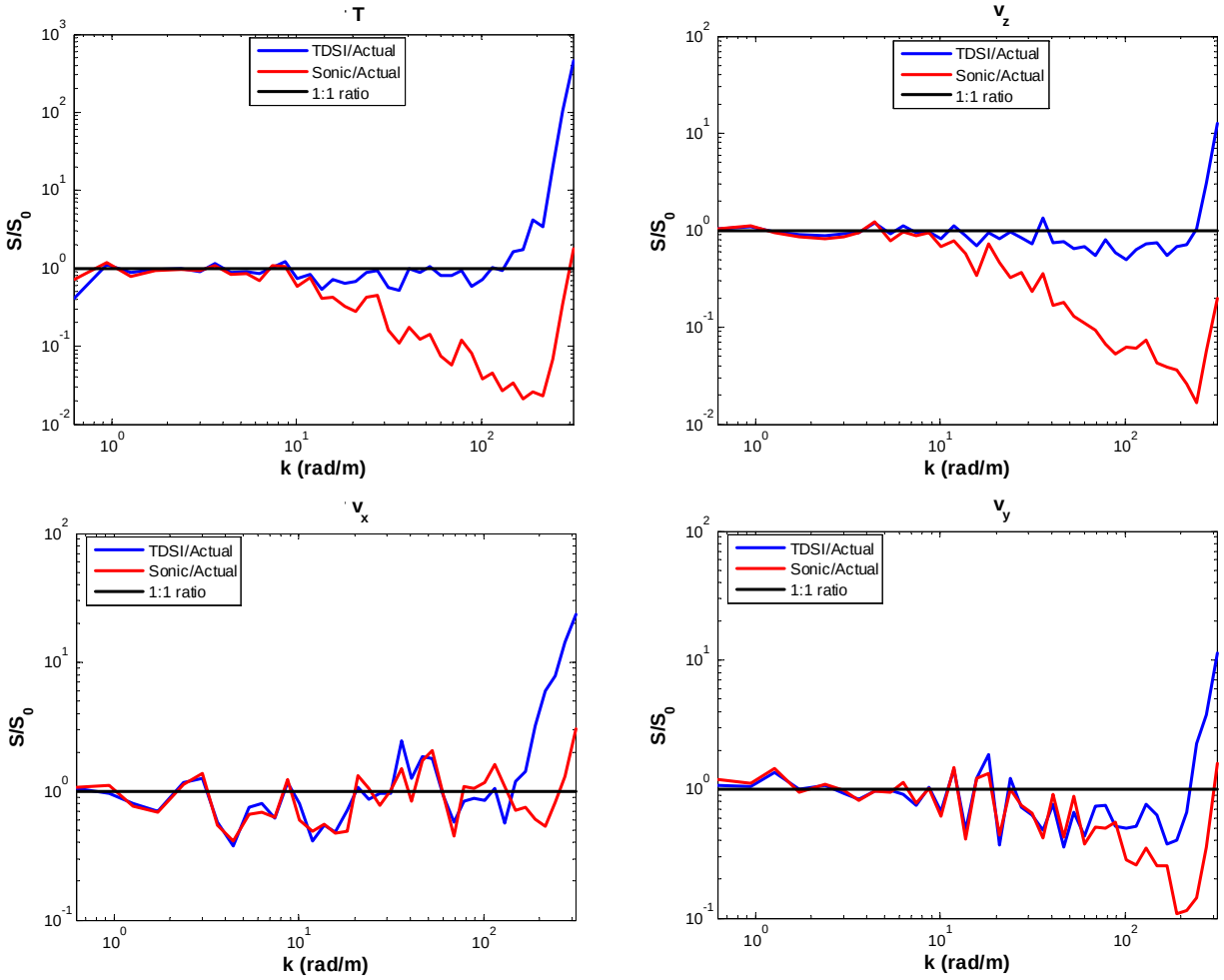

Figure 8: Normalized spectra of T fluctuations (upper left), v_z fluctuations (upper right), v_x fluctuations (lower left), and v_y fluctuations (lower right) reconstructed in numerical simulations of the sonic anemometer (red lines) and its suggested modification (blue lines). The spectra are normalized by the corresponding QW spectra. The black, horizontal lines correspond to a perfect reconstruction of the spectra.